Equivalence of grounded and non-grounded NES's tuning and performance in mitigating transient vibrations

Kevin Dekemele[1], Lennert De Knop[1] Patrick Van Torre[2], and Mia Loccufier[1]

[1] Ghent University, Department of Electromechanical, Systems and Metal engineering, Technologiepark-Zwijnaarde 125, Ghent, Belgium
kevin.dekemele@ugent.be,
[2] Ghent University, Department of Information Technology, Technologiepark-Zwijnaarde 126, Ghent, Belgium

Abstract. Nonlinear energy sinks serve as more robust vibration absorbers than linear counterparts. In literature, the most popular NES is the non-grounded NES (NGNES), a mass connected to a vibrating mechanical system through a highly nonlinear spring. Less known are the grounded NESs (GNES), that are connected to the mechanical system through a weak linear spring, and grounded through a highly nonlinear spring. To increase the performance of the NGNESs, its mass may be increased. However, as the NGNES's mass rests on mechanical system, this NES's mass is typically limited to a light-weight. On the other hand, GNES design is not limited by its mass as it rests on the ground. Furthermore, the weak connecting spring increases the design flexibility compared to the NGNES. In this contribution, it will be shown that tuning and performance prediction of the GNES performance is highly similar as previously discovered for the NGNES while showing there is more design flexbility for the GNES.

Keywords: nonlinear energy sink, vibration absorber

1 Introduction

When a nonlinear nonlinear energy sink (NES) is attached to a mechanical system, the vibration energy is irreversibly transferred from the mechanical system to the NES through targeted energy transfer (TET). This occurs because of highly localized nonlinear normal modes, where the vibration energy is mainly localized in the NES. The first research about these NESs focussed on grounded NESs (GNESs) (Figure 1a). It was investigated in the context of the redistribution of energy between a highly nonlinear and a linear oscillator, connected by a weak linear stiffness [1]. Later, non-grounded NESs (NGNESs) (Figure 1b) were given more attention in literature, primarily as vibration absorbers [2]. As a NGNES rests on the vibrating mechanical system, the NES mass is typically only a fraction of the mechanical system, e.g. 2 %. Yet in [3], it was shown that increasing the NES mass expedited vibration transfer. GNESs do not have this limitation, and additionally have more design freedom with the weak connecting spring. In engineering applications, the NGNES has been widely applied to civil structures [4], (rotating) machinery [5, 6] and aerospace [7] but GNES applications are few and far between. In [8], a GNES was developed to suppress lateral vibrations in a rotor system. An equivalent GNES model also appears when shunting piezoelectric material with a nonlinear impedance for vibration absorption [9]. In the research presented here, the GNES's dynamics will be analyzed by deriving its slow invariant manifold (SIM), expressing the evolution of the vibrations envelope on a slow time scale. The contributions are 1) the SIM is found to be equivalent to the SIM derived for the NGNES in [3], 2) the GNES performance can be predicted from simple formulae that solely depend on properties of the mechanical system and GNES, 3) the introduction of a novel *beating* measure, expressing the degree of back-and-forth vibration reflection between the GNES and the mechanical system, and 4) a tuning methodology based on maximizing GNES performance by increasing mitigation speed while steering clear of beating.

The paper is structured in the following manner: in the next section, the SIM for the GNES is derived and compared to NGNES's SIM. Then in section 3, analytical performance measures are derived, expressing the mitigation speed, dissipated energy and beating. Section 4 presents the novel tuning methodology balancing the aforementioned performance measure and finally in section 5 the conclusions are made.

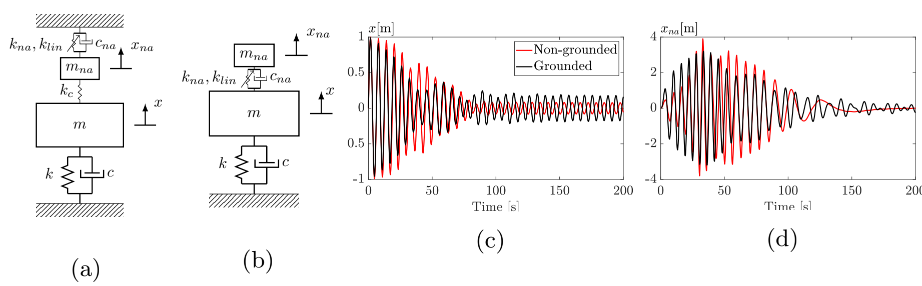

Fig. 1: The grounded (a) and non-grounded (b) NES coupled to an SDOF system. Mechanical system's (c) and NES's vibrations (d).

2 System Dynamics

The dynamics of a GNES coupled to a mechanical system (Figure 1a) is described by the following differential equations:

$$\begin{cases} m\ddot{x} + c\dot{x} + kx + k_c(x - x_{na}) = 0 \\ m_{na}\ddot{x}_{na} + c_{na}\dot{x}_{na} + k_{na}x_{na}^3 + k_{lin}x_{na} + k_c(x - x_{na}) = 0 \end{cases} \tag{1}$$

Similarly for the NGNES:

$$\begin{cases} m\ddot{x} + c\dot{x} + kx + c_{na}(\dot{x} - \dot{x}_{na}) + k_{na}(x - x_{na})^3 + k_{lin}(x - x_{na}) = 0 \\ m_{na}\ddot{x}_{na} + c_{na}(\dot{x}_{na} - \dot{x}) + k_{na}(x_{na} - x)^3 + k_{lin}(x_{na} - x) = 0 \end{cases} \tag{2}$$

A first numerical simulation is presented in Figures 1c and 1d. Here the mechanical system has a mass $m = 1$ kg, a stiffness $k = 1$ N/m and no damping. It has an initial speed of $x(0) = 1$ m/s. The NGNES has a NES mass $m_{na} = 0.02$ kg, a damping $c_{na} = 0.002$ Ns/m, and a cubic nonlinear stiffness of $k_{na} = 0.004$ N/m^3 and the GNES $m_{na} = 0.04$ kg, $c_{na} = 0.002$ Ns/m, and $k_{na} = 0.004$ N/m^3. For this particular set of parameters, the vibrations are highly similar. The vibrations in the mechanical system decrease until about 70 s, after which a residual amount of energy is dissipated very slowly, typical of NESs. To clarify why they are similar, the SIM for both the GNES and NGNES are derived next.

2.1 Grounded absorber

Dividing (1) by mass m yields

$$\begin{cases} \ddot{x} + \epsilon\lambda\dot{x} + \omega_0^2 x + \epsilon\omega_0^2(x - x_{na}) = 0 \\ \epsilon\mu\ddot{x}_{na} + \epsilon\lambda_{na}\dot{x}_{na} + \epsilon\Omega_3\omega_0^4 x_{na}^3 + \epsilon\kappa\omega_0^2 x_{na} + \epsilon\omega_0^2(x_{na} - x) = 0 \end{cases}$$

where

$$\begin{aligned} \epsilon\lambda = \frac{c}{m} \quad \omega_0^2 = \frac{k}{m} \quad \epsilon = \frac{k_c}{k} \quad \mu = \frac{m_{na}}{k_c}\omega_0^2 \\ \kappa = \frac{k_{lin}}{k_c} \quad \lambda_{na} = \frac{c_{na}}{k_c}\omega_0^2 \quad \Omega_3 = \frac{k_{na}}{k_c\omega_0^2} \end{aligned} \tag{3}$$

with $\epsilon \ll 1$. For $\kappa < -\frac{1}{1+\epsilon}$, the NES is bistable. Bistable NESs have two stable resting positions where $x \neq 0$ and $x_{na} \neq 0$, which may strain the system at rest. Furthermore, unoptimal chaotic vibrations may occur [10]. This will not be considered in this paper.

The slow flow dynamics are obtained by applying the following steps:

- A 1:1 resonance with frequency ω_0 is assumed.
- A complexification of the dynamic variables to $\varphi(t)e^{j\omega_0 t} = \dot{x} + j\omega_0 x$ and $\varphi_{na}(t)e^{j\omega_0 t} = \dot{x}_{na} + j\omega_0 x_{na}$ is applied with φ_{na} and $\varphi \in \mathbb{C}$ the dynamic envelopes.
- The complex variables are expressed as a perturbation series in ϵ, $\varphi = \varphi_0 + \epsilon\varphi_1$ and $\varphi_{na} = \varphi_{na,0} + \epsilon\varphi_{na,1}$.
- The dynamics are regarded on two time scales, $T_0 = t$, the fast time, and $T_1 = \epsilon t$, the slow time.
- The complex, slow time variables are expressed in their polar notation : $\varphi_0(T_1) = R_0 e^{j\delta_0}$ and $\varphi_{na,0}(T_1) = R_{na}e^{j\delta_{na}}$.

- Dimensionless envelope variables $Z_0 = \Omega_3 E_0$ and $Z_{na} = \Omega_3 E_{na}$ are introduced, with $E_0 = R_0^2 = |\varphi_0(T_1)|^2$ and $E_{na} = R_{na}^2 = |\varphi_{na}(T_1)|^2$.
- Damping is made dimensionless with $\xi = \frac{\lambda}{\omega_0}$ and $\xi_{na} = \frac{\lambda_{na}}{\omega_0}$.

A more thorough derivation is found in [3]. While applying these steps, all terms $\mathcal{O}(\epsilon^2)$ were neglected.

The result is the slow flow dynamics:

$$\begin{aligned} \frac{\partial Z_0}{\partial T_1} &= -\lambda Z_0 - \lambda_{na} Z_{na} \\ Z_0 &= \left[\xi_{na}^2 + \left(\mu - \kappa - 1 - \frac{3}{4} Z_{na}\right)^2\right] Z_{na} \end{aligned} \tag{4}$$

The set of equations in (4) have a dynamic and static relation between the dimensionless envelope of the mechanical system Z_0 and the NES's vibration Z_{na}. The dynamic relation dictates that Z_0 decreases if there is damping (λ and λ_{na}). The static relation is called the slow invariant manifold (SIM) and constrains the relation between Z_{na} and Z_0. Next, the SIM for the NGNES is derived.

2.2 Non-grounded absorber

Dividing (2) by mass m:

$$\begin{cases} \ddot{x} + \epsilon\lambda\dot{x} + \omega_0^2 x + \epsilon\ddot{x}_{na} = 0 \\ \epsilon\ddot{x}_{na} + \epsilon\lambda_{na}(\dot{x}_{na} - \dot{x}) + \epsilon\Omega_3\omega_0^4(x_{na} - x)^3 + \epsilon\kappa\omega_0^2(x_{na} - x) = 0 \end{cases} \tag{5}$$

with

$$\begin{aligned} \epsilon\lambda &= \frac{c}{m} \quad \omega_0^2 = \frac{k}{m} \quad \epsilon = \frac{m_{na}}{m} \\ \kappa &= \frac{k_{lin}}{m_{na}\omega_0^2} \quad \lambda_{na} = \frac{c_{na}}{m_{na}} \quad \Omega_3 = \frac{k_{na}}{m_{na}\omega_0^4} \end{aligned} \tag{6}$$

Although these parameters share the same symbols as in (3), their physical meaning are different.

To derive the slow flow dynamics, similar steps are applied as above, except the complexified variables are now defined as $\varphi(t)e^{j\omega_0 t} = \dot{x} + \epsilon\dot{x}_{na} + j\omega_0(x + \epsilon x_{na})$ and $\varphi_{na}(t)e^{j\omega_0 t} = \dot{x}_{na} - \dot{x} + j\omega_0(x_{na} - x)$. The slow flow dynamics for the NGNES are:

$$\begin{aligned} \frac{\partial Z_0}{\partial T_1} &= -\lambda Z_0 - \lambda_{na} Z_{na} \\ Z_0 &= \left[\xi_{na}^2 + \left(1 - \kappa - \frac{3}{4} Z_{na}\right)^2\right] Z_{na} \end{aligned} \tag{7}$$

The dynamic relation is equivalent as in (4) while the SIM is slightly different. The SIM is now generalized for both NESs.

2.3 Slow dynamics

The slow flow dynamics and SIM for both NESs, (4) and (7) are generalized as:

$$\begin{aligned} \frac{\partial Z_0}{\partial T_1} &= -\lambda Z_0 - \lambda_{na} Z_{na} \\ Z_0 &= \left[\xi_{na}^2 + \left(\Gamma - \frac{3}{4} Z_{na}\right)^2\right] Z_{na} \end{aligned} \tag{8}$$

with $\Gamma = 1-\kappa$ for the non-grounded absorber, and $\Gamma = \mu-\kappa-1$ for the grounded absorber. Note that the dimensionless constants have a different physical meaning for the GNES (3) and NGNES (6). The simulations in Figures 1c and 1d are compared to their slow flow dynamics in Figure 2. For the GNES, $\mu = 2$ and $\kappa = 0$ and for the NGNES $\kappa = 0$. Thus for both NESs $\Gamma = 1$, $\xi_{na} = 0.1$ and $Z_0(0) = 0.2020$, and as such their SIM and slow flow evolutions are equivalent. The actual vibrations of the NESs follow the slow flow on average. The SIM as seen in Figure 2c has a fold and two local extrema:

$$\begin{cases} Z_{na\pm} = \dfrac{4}{9}\left(2\Gamma \pm \sqrt{\Gamma^2 - 3\xi_{na}^2}\right) \\ Z_0^{\pm} = \left[\xi_{na}^2 + \left(\Gamma - \dfrac{3}{4} Z_{na\mp}\right)^2\right] Z^{na\mp} \end{cases} \tag{9}$$

with $\{Z_0^+, Z_{na}^-\}$ a local maximum and $\{Z_0^-, Z_{na}^+\}$ a local minimum which exist for:

$$\xi_{na} < \frac{\Gamma}{\sqrt{3}} \tag{10}$$

The condition (10) for the existence of the extrema and thus the fold is required for efficient energy transfer [3, 10]. Optimal energy transfer occurs when the dynamics initiate on the right branch of the SIM, where according to the dynamic relation of (8), the decay rate of Z_0 is the highest. The SIM also has a local minimum. The vibrations decay efficiently to the minimum and then jump to the left branch. This explains the residual energy.

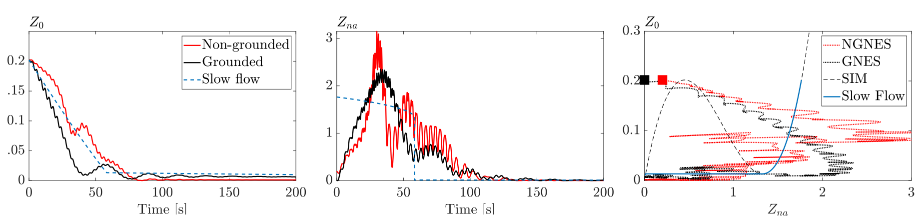

(a) (b) (c)

Fig. 2: Comparison of slow flow dynamics and simulations of complete dynamics.

3 Performance

Observing the slow flow evolution in Figure 2 reveals that Z_0 decays almost linearly at a high rate until a change of slope. The remaining Z_0 after the slope change is the residual energy which is dissipated for slowly. At the same time, Z_{na} drops to a low value. On the SIM in Figure 2c, this drop in NES efficiency corresponds to the jump from the right branch to the left branch. Now, simple analytic formulae expressing the duration of efficient energy transfer (or pumping time) and the residual energy are derived from (8).

3.1 Analytical performance measures

Residual energy The residual energy is the vibration energy left after the slow flow dynamics jump from the right to the left branch. Relative to the initial energy, it is found as:

$$E_{res} = \frac{Z_0^-}{Z_0(0)} = \frac{E_0^-}{E_0(0)} \tag{11}$$

These energy measures are calculated from the compound system's parameters (9), and the initial energy , $Z_0(0) = \Omega_3(\dot{x}(0)^2 + \omega_0^2 x^2(0))$.

Pumping time From (4) the expression for $\frac{\partial Z_{na}}{\partial T_1}$ can be determined. By neglecting system damping, $\xi \approx 0$, the expression is integrated to obtain:

$$\overbrace{\frac{27}{32} Z_{na}^2 - 3\Gamma Z_{na} + \left(\Gamma^2 + \xi_{na}^2\right) \ln(Z_{na})}^{I(Z_{na})} = C - \omega_0 \xi_{na} T_1 \tag{12}$$

The duration between two values of Z_{na} can be calculated from (12). The pumping time can then we calculated as:

$$\epsilon T_{pump} = \frac{1}{\omega_0 \xi_{na}} \left(I(Z_{na}(0)) - I(Z_{na}^+) \right) \tag{13}$$

This expression also only depends on the compound system's parameters and the initial energy. Here $Z_{na}(0)$ is the value on the right branch corresponding with $Z_0(0)$. The pumping time is inversely proportional to ϵ. For the NGNES this is the mass ratio, which has hard upper limit. For the GNES this is the stiffness ratio, which does not have a hard constraint.

Prediction of performance For the coefficient and initial conditions of simulations in Figure 1 and Figure 2, the pumping time T_{pump} is 58.2 s and the residual energy is 0.066. These can be calculated before a numerical simulation, to predict the the performance.

3.2 Beating index

A vibration consisting of two closely spaced frequencies ω_1 and ω_2 has a significant amplitude modulating beat of frequency $\frac{\omega_2-\omega_1}{2}$. In the simulations in Figure 1, the GNES shows some slight beating, where vibration energy is reflected back-and-forth from NES to mechanical system.

The linear eigenfrequencies of the grounded absorber are derived from the following determinant, obtained from a linearized version of (1):

$$\begin{vmatrix} (1+\epsilon)\omega_0^2-\omega^2 & -\epsilon\omega_0^2 \\ -\epsilon\omega_0^2 & \epsilon\omega_0^2(1+\kappa)-\epsilon\mu\omega^2 \end{vmatrix} = 0$$
$$\Longrightarrow \omega^2 = \frac{1+\mu(1+\epsilon)+\kappa \pm \sqrt{(1+\mu(1+\epsilon)+\kappa)^2-4\mu(1+\kappa+\epsilon\kappa)}}{2\mu}\omega_0^2 \tag{14}$$
$$\approx \frac{1+\mu+\kappa\pm(\mu-1-\kappa)}{2\mu}\omega_0^2 \Rightarrow \omega_{1,2}^2 \approx \{\frac{1+\kappa}{\mu},1\}\cdot\omega_0^2$$

Similar, for the non-grounded absorber:

$$\begin{vmatrix} (1+\epsilon\kappa)\omega_0^2-\omega^2 & -\epsilon\kappa\omega_0^2 \\ -\epsilon\kappa\omega_0^2 & \epsilon\kappa\omega_0^2-\epsilon\omega^2 \end{vmatrix} = 0 \Longrightarrow \quad \omega_{1,2}^2 = \{\kappa,1\}\cdot\omega_0^2 \tag{15}$$

The following measures expresses the proximity of the eigenfrequencies:

$$I_{beat}^2 = \frac{\omega_2^2-\omega_1^2}{\omega_0^2} \overset{\text{GNES}}{=} \frac{\mu-\kappa-1}{\mu} \quad \overset{\text{NGNES}}{=} 1-\kappa \tag{16}$$

For the simulation in Figure 1, I_{beat}^2 is 0.5 for the GNES and 1 for the NGNES. The linearized eigenfrequencies for the GNES are closer, explaining the *higher degree of beating* in the GNES.

4 Tuning

Although the GNES and NGNES have an equivalent SIM and performance measures, tuning and designing the physical parameters of both NESs is different. While the NGNES has a hard constraint on the absorber mass, directly impacting ϵ and thus the performance (it is in the denominator in (13)), this is less of an issue for the GNES. Moreover, the ϵ for the GNES, the stiffness ratio, generally does not have a hard constraint. The only real tuning parameters for the NGNES are thus the damping ξ_{na} and κ. For the GNES, ϵ, μ, κ and ξ_{na} can be considered to be design parameters. However, this high dimensional design space increases the complexity of finding suitable GNES parameters. Therefore, a novel tuning methodology is presented next.

4.1 Tuning plane GNES

To obtain a suitable choice for μ and κ, the tuning plane is presented in Figure 3. The choice for μ and κ is constrained by the conditions for the fold in the SIM, (10), $\mu > \kappa + 1 + \sqrt{3}\xi_{na}$, by the condition for bistability and chaotic vibrations $\kappa > -\frac{1}{1\epsilon}$ and by an optional mass constraint $\mu < \mu_{max}$. These constraints form a triangle of admissible μ and κ values, within the black lines in Figure 3.

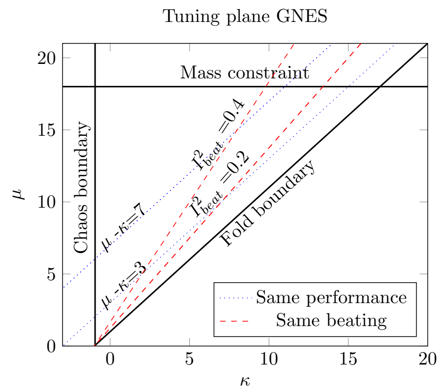

Fig. 3: Tuning plane for grounded NES for $\epsilon = .02$ and $\xi_{na} = 0.1$.

The class of GNESs with equal Γ, or where $\mu - \kappa = C$, $C > 1$ have the same analytical performance, (13) and (11). Two equi-performance lines are drawn on Figure 3. Additionally, lines for constant beating index, $\mu = \frac{1+\kappa}{1-I^2_{beat}}$ are also shown. For the same predicted performance, GNES more to the right on the tuning plane suffer more from beating.

4.2 Simulations

For the mechanical system presented in section 2, several GNESs are now tuned, with parameters given in Table 1. Each time, Ω_3 is chosen such that $Z_0(0) = 2{\cdot}Z_0^+$ to ensure the dynamics attract to the right branch of the SIM. Five NES will be simulated for $\dot{x}(0) = 1$ m/s. The first two NESs, where $\mu - \kappa = 4$, lay on a equi-performance line, but have a different beating index. The simulations in Figures 4a and 4d reveal a similar performance, but significant beating for the second NES. The next 2 NESs have $\mu - \kappa = 2$, a faster GNES is predicted with the pumping time and is confirmed in Figures 4b and 4e. However, The NES with the lower beating index, has significantly more residual energy in the simulation, not predicted by (11). From these simulations, one might suggest that an as small $\mu - \kappa$ with an as small μ is the optimal choice. As a counterexample, NES 5 is simulated, having an $\epsilon = 0.12$ and a $\mu = 4$, or $m_{na} = 0.48$. It is compared to NES 3 in Figures 4c and 4f and has comparable performance. Additionally, NES 5 has a lower stroke. The high absorber mass of this NES, 0.48 kg, would not be feasible for NGNESs.

	Ω_3	μ	κ	ϵ	E_{res}	T_{pmp}	I^2_{beat}
1	10.7	4	0	0.02	0.003	1021 s	0.75
2	10.7	24	20	0.02	0.003	1021 s	0.125
3	0.404	1.1	-0.9	0.02	0.03	112 s	0.9
4	0.404	5	3	0.02	0.03	112 s	0.2
5	10.7	4	0	0.12	0.003	170 s	0.75

Table 1: NES parameters and static performance.

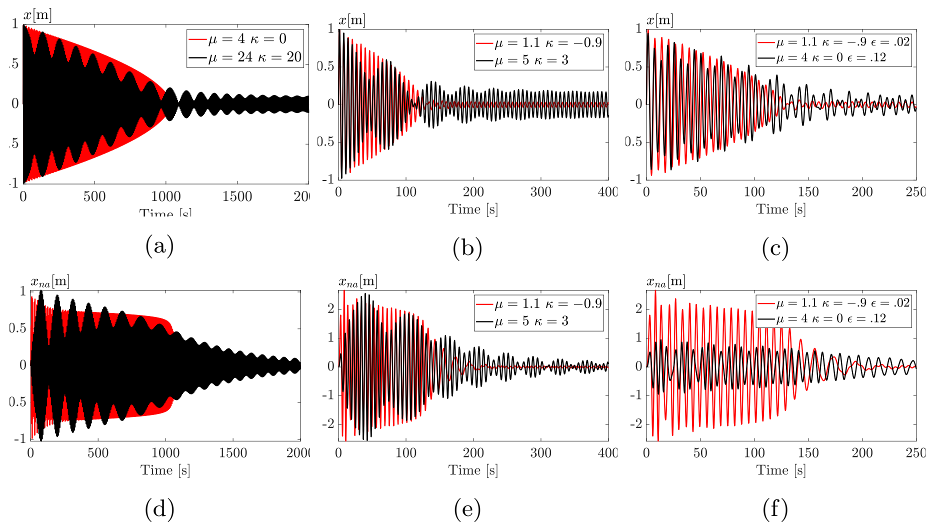

Fig. 4: Simulation of NES in Table 1, NESs 1 and 2 (a)(d), 3 and 4 (b)(e) and 3 and 5 (c)(f).

5 Conclusion

This paper presented a thorough research of the grounded nonlinear energy sink (GNES) based on its slow invariant manifold (SIM). It was shown that the SIM has an equivalent shape as the SIM of non-grounded NESs, but where the GNES mass and coupling spring have a different role. The performance of the GNES could be predicted with static performance measures and the novel beating index. These allowed to construct a tuning plane GNES, constrained by constant lines of performance and beating. It was shown that for GNESs with distant linear eigenfrequencies or a high beating index, the static performance measure are good predictors of the duration of energy transfer and residual energy. The opposite was true GNESs with close eigenfrequencies or low beating index. The increased design freedom of the GNES allows a performant vibration mitigation for both a small NES mass with weak coupling spring and higher NES mass with stronger coupling spring. The latter configuration has a smaller stroke.

Bibliography

[1] Oleg V Gendelman. Transition of energy to a nonlinear localized mode in a highly asymmetric system of two oscillators. *Nonlinear Dynamics*, 25(1-3):237–253, 2001.

[2] Gaetan Kerschen, Young Sup Lee, Alexander F Vakakis, D Michael McFarland, and Lawrence A Bergman. Irreversible passive energy transfer in coupled oscillators with essential nonlinearity. *SIAM Journal on Applied Mathematics*, 66(2):648–679, 2005.

[3] Kevin Dekemele, Robin De Keyser, and Mia Loccufier. Performance measures for targeted energy transfer and resonance capture cascading in nonlinear energy sinks. *Nonlinear Dynamics*, 93(2):259–284, 2018.

[4] S Lo Feudo, C Touzé, Jean Boisson, and G Cumunel. Nonlinear magnetic vibration absorber for passive control of a multi–storey structure. *Journal of Sound and Vibration*, 438:33–53, 2019.

[5] G Habib, Gaëtan Kerschen, and Gabor Stepan. Chatter mitigation using the nonlinear tuned vibration absorber. *International Journal of Non-Linear Mechanics*, 91:103–112, 2017.

[6] A Haris, Panagiotis Alevras, Mahdi Mohammadpour, Stephanos Theodossiades, and M O'Mahony. Design and validation of a nonlinear vibration absorber to attenuate torsional oscillations of propulsion systems. *Nonlinear Dynamics*, pages 1–17, 2020.

[7] Baptiste Bergeot, Sergio Bellizzi, and Bruno Cochelin. Passive suppression of helicopter ground resonance using nonlinear energy sinks attached on the helicopter blades. *Journal of Sound and Vibration*, 392:41–55, 2017.

[8] Hongliang Yao, Yanbo Cao, Zhiyu Ding, and Bangchun Wen. Using grounded nonlinear energy sinks to suppress lateral vibration in rotor systems. *Mechanical Systems and Signal Processing*, 124:237–253, 2019.

[9] Régis Viguié, Gaëtan Kerschen, and M Ruzzene. Exploration of nonlinear shunting strategies as effective vibration absorbers. In *Active and Passive Smart Structures and Integrated Systems 2009*, volume 7288, page 72882B. International Society for Optics and Photonics, 2009.

[10] Kevin Dekemele, Patrick Van Torre, and Mia Loccufier. Performance and tuning of a chaotic bi-stable nes to mitigate transient vibrations. *Nonlinear Dynamics*, 98(3):1831–1851, 2019.